Main Manuscript for

A Zinc finger (ZnF) transcription factor exerts its multifaceted function through ZnF-regulated phase separation

Yatao Chen[1], Yajie Wan[1], Xiaoying Pei[1], Tan Wang[1], Zhifang Ma[1], Liming Chen[1], [2], *.

[1]Department of Biochemistry, School of Life Sciences, Nanjing Normal University, Nanjing, China; [2]Cancer Institute, School of Life Sciences, Nanjing Normal University, Nanjing, China

[*] Corresponding author: Liming Chen;

Email: chenliming1981@njnu.edu.cn

Author Contributions: L. C. conceived the project; L.C. and Y.C designed research; Y.C, Y.W, X.P, T.W and Z.M performed research; Y.C and L.C analyzed data; Y.C and L.C wrote the paper. L.C. was responsible for research supervision.

Competing Interest Statement: The authors declare no conflicts of interest.

Classification: Biology

Keywords: zinc finger, transcription factor, liquid-liquid phase separation, GATA3, breast cancer-associated mutations, immune

This PDF file includes:

Main Text
Figures 1 to 5

Abstract

Zinc finger (ZnF) transcription factors (TFs) consist of ZnF-containing DNA-binding domains (DBDs) and intrinsically disordered region (IDR)-containing activation domains (ADs). Recent studies suggest that liquid-liquid phase separation (LLPS) is the fundamental mechanism underlying human health and disease, with ZnF TFs activating gene expression through the LLPS capacity of their IDR-containing ADs. However, little is known about how the well-folded DBD of ZnF TFs might be involved in their LLPS mechanism. *GATA3* has been identified as one of the most frequently mutated genes in breast cancer, and its encoded protein GATA3, which contains two ZnFs (ZnF1 and ZnF2) in its DBD, is a master regulator of immunity. Here, we show that GATA3 undergoes LLPS in cells and *in vitro*, with its DBD playing an important regulatory role. Mechanistically, ZnF2 in the DBD contains two arginine amino acids (R329 and R330) to provide the critical charges to regulate GATA3 LLPS by generating multivalent electrostatic interactions. Functionally, we demonstrated that ZnF2-regulated GATA3 LLPS is the mechanism underlying the multifaceted function of GATA3 in breast cancer development and immune regulation, where aberrant GATA3 LLPS caused by artificial or breast cancer-associated ZnF2-defective mutations showed significantly reduced potentials in promoting breast cancer development and exhibited remarkably enhanced capacities in activating type I interferon signaling. Since ZnF is a common feature in the DBDs of ZnF TFs, by describing GATA3 as a proof-of-principle, our data suggest that ZnF-regulated LLPS may be a general mechanism underlying the multifaceted function of ZnF TFs in human health and disease.

Significance Statement

Zinc finger (ZnF) transcription factors (TFs), the most prominent TFs in humans, play critical roles in human health and disease. The ZnF TF GATA3 is important for breast cancer development and immune regulation. Here, we show that GATA3 undergoes liquid-liquid phase separation (LLPS), which is regulated by its well-structured DNA-binding domain, specifically ZnF2. We demonstrate that ZnF2-regulated LLPS is a phenotype-associated mechanism underlying the multifaceted functions of GATA3 in breast cancer development and immune regulation. This study reports GATA3 as a proof-of-principle to reveal a previously unrecognized mechanism that can potentially be generalized to improve the mechanistic understanding of the multifaceted function of ZnF TFs in various human health and disease settings, including the complex diseases such as cancer.

Main Text

Introduction

Transcription factors (TFs) are characterized by consisting of one or more well-folded DNA-binding domains (DBDs) and activation domains (ADs). Most prominent TFs in human contain Zinc fingers (ZnFs) in their DBDs, known as ZnF TFs, play multifaceted function in regulating various critical biological processes underlying human health and diseases (1, 2). Recent evidence suggests that liquid-liquid phase separation (LLPS) is a phenotype-associated mechanism underlying human health and disease (3). The intrinsically disordered regions (IDRs) in protein sequences are considered to be the driving force for protein LLPS (4). Previous studies have characterized that some Zn TFs, such as OCT4 and GCN4, activate their target genes through the phase-separation capacity of their IDR-containing ADs (5). LLPS research is still in its infancy and requires further investigation to translate our current knowledge of LLPS into novel mechanistic, functional and therapeutic discoveries. For ZnF TFs, little is known about how well-folded DBDs of ZnF TFs and the ZnFs in their DBDs might be involved in their LLPS-mediated mechanisms underlying human health and disease, such as cancer.

GATA TF family, an important Zn TF family consisting of six ZnF TFs (GATA1-6), has been well characterized to be involved in a variety of physiological and pathological processes, and many disease-associated mutations are located in and around the ZnF regions (6). GATA3, encoded by

the *GATA3* gene, is a typical member of the GATA TF family, and its DBD contains two ZnFs: ZnF1 and ZnF2. Studies in animal models and humans have characterized the important roles of GATA3 in controlling the expression of a wide range of biologically and clinically important genes. Elevated GATA3 expression were found in various cancers, including breast cancer (7). In particular, *GATA3* is among the top 3 most frequently mutated genes in breast cancer (8), and GATA3 is a master regulator in immunity (9). In this study, we intended to investigate GATA3 to conceptually argue the role and mechanism of the DBD and its ZnFs in the LLPS-mediated multifaceted function of ZnF TFs in human health and disease.

We found that GATA3 undergoes LLPS in cells and *in vitro*. In GATA3 LLPS, its N-terminal domain (N), known as its AD, but not its C-terminal domain, is likely to play a driving role by containing IDRs, and its DBD, specifically ZnF2 but not ZnF1 in its DBD, plays an important regulatory role by containing two arginine amino acids: R329 and R330. In contrast to the IDRs in GATA3 AD, which contribute to LLPS through different types of multivalent interactions, ZnF2 in the GATA3 DBD regulates LLPS through multivalent electrostatic interactions (MEIs), with R329 and R330 in ZnF2 providing important charge blocks. Aberrant LLPS caused by mutations in and around R329 and R330, including both artificial and breast cancer-associated mutations, showed reduced oncogenic potential in promoting breast tumor growth, and enhanced the expression of immune genes in breast cancer cells, mainly interferon-stimulated genes (ISGs) for interferon (IFN) signaling. These data suggest that ZnF2 modulates the multifaceted function of GATA3 in breast cancer development and immune regulation through regulating the LLPS of GATA3. Since charged amino acid-containing ZnFs with the intrinsic ability to generate MEIs are a common feature of ZnF TFs, GATA3 may serve as a proof-of-principle to suggest that LLPS regulated by ZnF-mediated MEIs is likely a general mechanism underlying the multifaceted function of ZnF TFs in many health and disease settings.

Results

LLPS capacity of GATA3 underlies its condensation on chromatin

ZnF TFs on chromatin, which appear as vital and ubiquitous condensates in cell nuclei, are tightly and dynamically regulated to control specific gene expression to modulate many important phenotype-related biological processes (10). Indeed, immunofluorescence (IF) assay revealed that GATA3 forms condensates on chromatin without colocalizing with non-chromatin condensation makers, including SC35, PML and Colin (Fig. 1 *A* and *B* and *SI Appendix,* Fig. S1*A*). 1,6-hexanediol treatment and Fluorescence Recovery After Photobleaching (FRAP) assay have been widely used to assess whether protein condensates are driven by LLPS-mediated assemblies (11). We found that GATA3-containing condensates on chromatin were disrupted upon 1,6-hexanediol treatment, and these condensates exhibited fluidity as evidenced by the fluorescence recovery after photobleaching in FRAP assays (Fig. 1 *C-E*). These results suggest the formation of GATA3-containing condensates on chromatin by the LLPS mechanism. GATA3-containing condensates on chromatin include many other proteins besides GATA3. To test whether GATA3 undergoes LLPS for its condensation on chromatin, we performed *in vitro* LLPS assays using purified recombinant GATA3 protein, which is MBP-GATA3 fusion protein and can be cleaved into GATA3 and MBP protein by the 3C prescission protease. In the turbidity assay, the results showed that MBP-GATA3 protein cleaved by protease 3C exhibited remarkable and significantly increased turbidity compared to the control (Fig. 1*F* and *SI Appendix,* Fig. S1*B*). In an *in vitro* droplet formation assay, both GATA3 with and without the mEGFP tag protein can form droplets (Fig. 1 *G* and *H*). Consistent with the observation in cells, 1,6-hexanediol treatment disrupts the droplets of purified GATA3-mGFP proteins, and FRAP assay showed that the fluorescence of GATA3-mGFP droplets can undergo fluorescence recovery after photobleaching (Fig. 1*I* and *SI Appendix*, Fig. S1*C*). Furthermore, the fusion event of GATA3 droplets was observed (Fig. 1*J*). These results suggest that GATA3 has LLPS capacity for its condensations on chromatin.

LLPS of GATA3 is regulated by its structured DBD

Zn TFs consist of structured DBDs containing ZnFs and ADs containing IDRs. For GATA3, its protein has a DBD that is flanked by two IDR-containing domains: N-terminal domain characterized as its AD and functionally-unknown C-terminal domain (Fig. 2*A*). We then intended

to investigate the role of different domains in the LLPS of GATA3. In both HEK293T and Hela cells, upon overexpression of wild type GATA3 ($GATA3^{WT}$) and its series of domain truncations, including N-terminal domain (AD), DBD, C-terminal domain (C), N-terminal domain truncation (△AD), DBD truncation (△DBD), and C-terminal domain truncation (△C), $GATA3^{WT}$, AD, DBD, △DBD, △AD, and △C, but not C, formed granules in cells, with only AD and AD-containing △DBD forming significantly more granules in cell nuclei compared to $GATA3^{WT}$ (Fig. 2 *B* and *C* and *SI Appendix* Fig. S2 *A*-C). Furthermore, in an *in vitro* droplet formation assay using purified proteins, the number of droplets formed by AD, DBD, △DBD, △AD, △C and C were all reduced compared to $GATA3^{WT}$ (Fig. 2*D*). Some Zn TFs, such as OCT4 and GCN4, have been characterized to activate their target genes through the phase-separation capacity of their IDR-containing ADs (5). Consistent with this, our results suggest that the IDR-containing AD but not C is likely to provide the driving force for GATA3 LLPS, while its DBD plays a regulatory role. Although not for Zn TFs, MEIs generated by charged amino acids have been characterized to be another important source of force for the LLPS of several proteins (12). Charge analysis revealed a remarkably higher average charge in the DBD of GATA3 compared to its AD and C (Fig. 2*E*). MEI-mediated LLPS can be attenuated with increasing salt concentration (13). We found that $GATA3^{WT}$ LLPS decreased with increasing NaCl concentration (Fig. 2 *F-G*). In addition, DBD, △AD and △C, which are GATA3 mutants containing DBD, but not △DBD, are sensitive to increasing NaCl concentration (Fig. 2*H* and *SI Appendix*, Fig. S2*D*). These results suggest that the structured DBD plays an important regulatory role in GATA3 LLPS through MEIs.

ZnF2 with its R329 and R330 is essential for the DBD in regulating GATA3 LLPS

For GATA3, its DBD with known DNA-binding complex structure contains two ZnFs: ZnF1 and ZnF2 (14). ZnF1 and ZnF2 have the highest average charges in the DBD of GATA3 by each containing two continuous charged arginine (R) amino acids (i.e. $R^{275}R^{276}$ in ZnF1 and $R^{329}R^{330}$ in ZnF2), which are shown to bind to DNA in the complex structure (Fig.3 *A* and *B*). To investigate whether and how $R^{275}R^{276}$ in ZnF1 and $R^{329}R^{330}$ in ZnF2 affect GATA3 LLPS, we generated another set of GATA3 mutants, including $GATA3^{4R\text{-}A}$ with the $R^{275}R^{276}$ in ZnF1 and $R^{329}R^{330}$ in ZnF2 all R mutated to alanine (A), $ZnF1^{2R\text{-}A}$ with the $R^{275}R^{276}$ in ZnF1 mutated to $A^{275}A^{276}$, and $ZnF2^{2R\text{-}A}$ with the $R^{329}R^{330}$ in ZnF2 mutated to $A^{329}A^{330}$. Interestingly, we found that $GATA3^{4R\text{-}A}$ and $ZnF2^{2R\text{-}A}$ but not $ZnF1^{2R\text{-}A}$ formed significantly more nuclear condensates in cells compared to $GATA3^{WT}$ (Fig. 3 *C* and *D*). Consistently, $ZnF2^{2R\text{-}A}$ shows altered LLPS compared to $GATA3^{WT}$ in an *in vitro* droplet formation assay (Fig. 1*H* and Fig. 3*E* and *SI Appendix* Fig. S3*A*). Although fusion events of $ZnF2^{2R\text{-}A}$ condensates were observed in cells, the fluorescence recovery of $ZnF2^{2R\text{-}A}$ condensates on chromatin in cells is significantly reduced compared to $GATA3^{WT}$ in FRAP assay (Fig. 3 *F* and *G* and *SI Appendix* Fig. S3*B*). The DBD of GATA3 is characterized by its specific binding to the DNA containing GATA-elements (15). In an *in vitro* droplet formation assay, we found that DNA containing GATA elements (GATA-DNA) but not DNA without GATA elements (noGATA-DNA), significantly altered the LLPS of both GATA3 (Fig. 3 *H* and *I*). In comparison, both GATA-DNA and noGATA-DNA can alter the LLPS of $ZnF2^{2R\text{-}A}$ (*SI Appendix* Fig. S3 *C* and *D*). Furthermore, FRAP assay results showed that GATA-DNA increased the fluidity of $GATA3^{WT}$ droplets but not $ZnF2^{2R\text{-}A}$ droplets compared to noGATA-DNA (Fig. 3 *J* and *K*). Taken together, these results suggest that ZnF2, but not ZnF1, is responsible for the regulatory role of DBD in GATA3 LLPS during the formation of GATA3 condensations on chromatin by recognizing GATA-containing genomic DNA in chromatin, where R329 and R330 in ZnF2 are the essential amino acids.

Aberrant LLPS of ZnF2-defective GATA3 mutants show reduced oncogenicity

GATA3 is one of the most frequently mutated genes in breast cancer (8). When we analyzed the gene mutation data archived in METABRIC (Molecular Taxonomy of Breast Cancer International Consortium), we found that in $GATA3^{mu}$ proteins encoded by breast cancer-associated *GATA3* mutations, ~40% of $GATA3^{mu}$ contain partially or completely defective ZnF2 ($ZnF2^{de}$), ~37% of $GATA3^{mu}$ contain intact ZnF2 ($ZnF2^{in}$), and the remaining ~23% of $GATA3^{mu}$ are highly variable (other mutations) (*SI Appendix*, Fig. S4*A*). To investigate whether breast-associated GATA3 mutants show aberrant LLPS behavior, four of the most frequently occurring mutants in the breast cancer were selected for further investigation, including two ZnF2-defective GATA3 mutants (a

splice mutation at X308-ZnF2$^{de\text{-}X308}$ and a frameshift mutation at R330-ZnF2$^{de\text{-}R330}$) and two ZnF2-intact GATA3 mutants (an M293K missense mutation-ZnF2$^{in\text{-}M293K}$ and a G360 truncation mutation -ZnF2$^{in\text{-}G360}$ (Fig. 4*A*). Similar to the artificial ZnF2-defective GATA3 mutant (ZnF2$^{2R\text{-}A}$) and the artificial ZnF2-intact GATA3 mutant (ZnF1$^{2R\text{-}A}$) described above, only overexpression of breast cancer-associated ZnF2-defective GATA3 mutants (ZnF2$^{de\text{-}X308}$ and ZnF2$^{de\text{-}R330}$) but not breast cancer-associated ZnF2-intact GATA3 mutants (ZnF2$^{in\text{-}M293K}$ and ZnF2$^{in\text{-}G360}$) formed significantly more nuclear condensations compared to GATA3^{WT} in HEK293T cells (Fig. 4 *B* and *C*). ZnF2$^{de\text{-}R308}$ condensations in cells can also be disassembled by 1,6-hexanediol treatment (Fig. 4*D*). Consistently, only overexpression of ZnF2-defective GATA3 mutants (and ZnF2$^{de\text{-}R330}$), but not ZnF2-intact GATA3 mutants (ZnF2$^{in\text{-}M293K}$ and ZnF2$^{in\text{-}G360}$), formed significantly more nuclear condensates compared to GATA3^{WT} in breast cancer cell lines, including T47D and MCF7$^{GATA3\text{-}KO}$ (Fig. 4*E* and *SI Appendix*, Fig. S4 *B* and *C*). These results suggest that ZnF2-regulated GATA3 LLPS may be a mechanism relevant to the development of breast cancer. To validate this suggestion, we first examined the relationship between the breast cancer-associated GATA3 mutants and the disease course of breast cancer. Consistent with the previous observations breast cancer patients with GATA3^{mu} show a better overall prognosis in ERα positive breast cancer patients compared to those with GATA3^{WT} (*SI Appendix*, Fig. S4*D*). Interestingly, breast cancer patients with ZnF2^{de} but not ZnF2^{in} mutations show a significantly better prognosis than those breast cancer patients with GATA3^{WT}, suggesting that ZnF2^{de} is the major contributor to the better prognosis of patients with GATA3^{mu} versus GATA3^{WT} (Fig. 4*F*). We then examined the effects of ZnF2^{de} on the development of breast cancer, we found that ZnF2-defective GATA3 mutants, including artificial ZnF2$^{2R\text{-}A}$ and breast cancer-associated ZnF2$^{de\text{-}X308}$ and ZnF2$^{de\text{-}R330}$, showed reduced oncogenic capacity in promoting tumor growth *in vitro* and *in vivo* compared to GATA3^{WT} (Fig. 4 *G-I*). Although GATA3 is considered to play important roles in breast cancer development, it's still under debate GATA3's controversial role in breast cancer: oncogene or tumor suppressor? (16) Both GATA3^{mu} and GATA3^{WT} are frequently upregulated in breast cancer (17). Our data suggest that elevated GATA3 in breast cancer, whether mutated or not, are oncogenic, while ZnF2-defective but not ZnF2-intact GATA3 mutants have significantly reduced oncogenic potential compared to wild-type GATA3 in promoting tumor growth by causing aberrant GATA3 LLPS, resulting in the better prognosis of patients with GATA3^{mu} compared to those with GATA3^{WT}.

Aberrant LLPS of ZnF2-defective GATA3 mutants enhances activation of IFN signaling

GATA3 has been characterized as a master immune regulator as shown by many studies performed in immune cells (9). Besides immune cells, increasing studies noticed essential roles of immune modulation in non-immune cells, such as cancer cells (18). However, the immune function of GATA3 in non-immune cells is largely unknown. To further argue that ZnF2-regulated GATA3 LLPS is an important mechanism underlying the multifaceted function of GATA3, we further investigated whether and how aberrant ZnF2-regulated GATA3 LLPS is also relevant to the immune events in breast cancer cells. To address this, we performed RNA-seq to examine the alteration of the transcriptional program by overexpression of ZnF2-defective GATA3 mutants, including artificial ZnF2$^{2R\text{-}A}$ and disease-associated ZnF2$^{de\text{-}X308}$ and ZnF2$^{de\text{-}R330}$, compared to overexpression of GATA3^{WT}, in MCF7$^{GATA3\text{-}KO}$ breast cancer cells. The results showed that in MCF7$^{GATA3\text{-}KO}$ cells, overexpression of ZnF2-defective GATA3 mutants significantly altered the cell transcriptional profiles compared to overexpression of GATA3^{WT} (Fig. 5*A* and *SI Appendix*, Table S1). Among the differentially expressed genes between a ZnF2-defective GATA3 mutant and GATA3^{WT}, there are 25 genes that consistently showed differential expression in ZnF2$^{2R\text{-}A}$, ZnF2$^{de\text{-}X308}$ and ZnF2$^{de\text{-}R330}$ compared to GATA3^{WT} (*SI Appendix*, Dataset S1 and Fig. S5*A*). Interestingly, 13 out of these 25 genes are immune genes, all of which were significantly upregulated in ZnF2-defective GATA3 mutants compared to GATA3^{WT} (Fig. 5*B*). Notably, 11 out of the 13 immune genes are ISGs, including *ISG15*, *IFI6*, *IFI27*, *IFI44L*, *IFIT1*, *IFIT3*, *IFI44*, *IFITM1*, *OAS2*, *OAS1* and *OASL*. Consistent with RNA-seq, RT-qPCR assay confirmed that all the 11 ISGs, were significantly upregulated by ZnF2-defective GATA3 mutants compared to GATA3^{WT}, suggesting a previously unrecognized important role of GATA3 in IFN signaling (Fig. 5*C* and *SI Appendix*, Fig. S5*B*). In support this suggestion, GSEA analysis revealed that positive

repose to type I IFN is consistently upregulated in $ZnF2^{2R-A}$, $ZnF2^{de-X308}$ and $ZnF2^{de-R330}$ compared to $GATA3^{WT}$ (Fig. 5*D*). IRF3 and TBK1 are key regulators in type I IFN signaling, the activation of which can be examined by the increased level of IRF3-S386 and IRF3-S396 phosphorylation (p-IRF3-S386 and p-IRF3-S396) and TBK1 (p-TBK1) (19). We found that overexpression of ZnF2-defective GATA3 mutants, such as $ZnF2^{de-X308}$ and $ZnF2^{de-R330}$, increased the levels of p-IRF3-S386, p-IRF3-S396 and p-TBK1 (Fig. 5*E*). In support of the more potent role of ZnF2-defective GATA3 mutants in activating type I IFN signaling compared to $GATA3^{WT}$, the expression levels of two type I IFN genes, *IFNA1* and *IFNB1*, were significantly increased in breast cancer cells overexpressing ZnF2-defective GATA3 mutants compared to those overexpressing $GATA3^{WT}$ (*SI Appendix,* Fig. S5*C*). These results suggest that ZnF2 and its $R^{329}R^{330}$ of GATA3 play an important role in innate immunity, specifically the activation of IFN signaling, in breast cancer cells.

It has been well characterized that ZnFs in the DBDs of ZnF TFs are essential for their binding to specific DNA-elements in chromatin to localize into chromatin subcompartments (CSCs) to control specific gene expression. CSCs positive for transcriptional activation markers, such as p300, which is typically recruited to transcriptional enhancers, and H3K27ac, which is an enhancer marker, are often under active transcription (20, 21). In support with ZnF2-defective GATA3 mutants in increasing the expression of ISGs compared to $GATA3^{WT}$ described above, IF assays showed that in $MCF7^{GATA3-KO}$ breast cancer cells, overexpression of ZnF2-defective GATA3 mutants, including artificial $ZnF2^{2R-A}$ and breast cancer-associated $ZnF2^{de-X308}$, increased their colocalization with p300-positive and H3K27ac-positive CSCs compared to $GATA3^{WT}$ (Fig. 5 *F* and *G*). In contrast to p300 and H3K27ac, H3K9me3 is associated with silencing of gene expression (22). Consistently, IF assays showed that in $MCF7^{GATA3-KO}$ breast cancer cells, the condensations of ZnF2-defective GATA3 mutants, including artificial $ZnF2^{2R-A}$ and breast cancer-associated $ZnF2^{de-X308}$, showed reduced H3K9me3 levels compared to $GATA3^{WT}$ (Fig. *5H*). Suv39H1 and SETDB1 are major histone lysine methyltransferases for the generation of H3K9me3 (23, 24). Consistently, in $MCF7^{GATA3-KO}$ breast cancer cells, overexpression of ZnF2-defective GATA3 mutants, including artificial $ZnF2^{2R-A}$ and breast cancer-associated $ZnF2^{de-X308}$ and $ZnF2^{de-R330}$, decreased suv39H1 but not SETDB1 protein levels and reduced H3K9me3 levels compared to $GATA3^{WT}$ (Fig. *5I*). Previous studies have identified ~3, 000 GATA3-bound genes with >14,000 GATA3 binding sites in immune cells (9, 10, 25). These GATA3-bound genes identified in immune cells include the ISGs, such as *IFIT3*, *OASL*, *IFIT1*, *IFI44L*, *IFI27* and *OAS1*, which were regulated by GATA3 in a ZnF2-mediated manner in breast cancer cells described above(26). In $MCF7^{GATA3-KO}$ breast cancer cells with overexpression of $GATA3^{WT}$, treatment with Chaetocin, an inhibitor of suv39H1 to disrupt H3K9me3 modification, increased GATA3 condensations on chromatin and the expression of ZnF2 defective mutants regulated above immune genes, which contains GATA3 bound ISGs, including *IFIT3*, *OASL*, *IFIT1*, *IFI44L*, *IFI27* and *OAS1*, compared to control (Fig. 5*J*). ZnF2-defective GATA3 mutants did not significantly alter the mRNA expression level of *suv39H1*, but significantly decreased the stability of suv39H1 protein compared to $GATA3^{WT}$, suggesting that ZnF2-defective GATA3 mutants decrease suv39H1 protein levels by destabilizing suv39H1 protein (*SI Appendix,* Fig. S5 *C-E*). CSCs are formed by an LLPS-mediated mechanism (11). It will be interesting to further investigate how ZnF2-defective GATA3 mutants destabilize suv39H1 proteins to regulate the LLPS-mediated formation of CSCs. Nevertheless, our data suggest that ZnF2-regulated LLPS regulates CSCs through suv39H1. When we examined the GATA3-bound genes in breast cancer cells with or without ZnF2-defective mutants by analyzing publicly available datasets, we found that in breast cancer cells, breast cancer-associated ZnF2-defective mutants, including $ZnF2^{de-X308}$ and $ZnF2^{de-R330}$, were remarkably more enriched on ISGs, such as *IFI6* and *IFI27*, compared to $GATA3^{WT}$ (*SI Appendix,* Fig. S5 *F* and *G*). Taken together, our results suggest that ZnF2-regulated LLPS is an important mechanism underlying GATA3 in controlling immune gene expression for immune regulation.

Discussion

ZnF TFs play important roles in cellular and organismal function or dysfunction in humans by controlling gene expression (1, 8). LLPS has now emerged as a fundamental mechanism underlying the precise regulation of various biological processes, including transcriptional regulation, which is the determinant molecular event underlying both the cellular and organismal phenotypic behaviors in human health and disease, including those related to cancer development (5, 27-29). LLPS of ZnF TFs has been suggested to be a driving mechanism underlying their functions in controlling gene transcription by characterizing some Zn TFs, such as Oct4 and GCN4, to activate their target genes via the LLPS capacity of their IDR-containing ADs (5), and GATA3 can undergo LLPS via the capacity of its IDR-containing AD (30). Besides the IDR-containing ADs, GATA3 and all other Zn TFs consist of ZnF-containing DBDs as their unique feature. The DBD of Zn TFs has the ability to bind DNA, where the ZnF in the DBDs play essential roles. However, it's largely unknown whether and how their well-folded DBDs and the ZnF in their DBDs can contribute to the LLPS of Zn-TFs. Here, we report that the structured DBD of GATA3 plays a master regulatory role in the LLPS of GATA3, where ZnF2 in the DBD and its R329 and R330 in the ZnF2 regulate the LLPS behavior of GATA3 by providing MEIs. By demonstrating aberrant LLPS of GATA3 upon mutation of its DBD of GATA3 or the ZnF2 in its DBD or R329 and R330 in the ZnF2, we claim that the DBD of a Zn TF and the ZnF in its DBD plays important role in MEI-mediated regulation of the LLPS capacity of its AD.

Cancers caused by gene mutations are a leading cause of human death, and breast cancer is the most common human cancer, with an estimated 2.3 million new cases in 2020 (31). In recent decades, extensive sequencing efforts have identified a large number of gene mutations in breast cancer and other major cancers (32). ZnF TFs, which are frequently mutated in cancer, play potentially critical roles in cancer initiation and progression (1). However, cancer-associated mutations of a given ZnF TF are myriad and lack functional and mechanistic interpretations. *GATA3* is one of the top 3 most frequently mutated genes in breast cancer (8). Previous studies have shown that breast cancer patients with $ZnF2^{de\text{-}X308}$ but not those with $ZnF2^{in\text{-}M293K}$ have a better prognosis than those with $GATA3^{WT}$ (33, 34). Another study showed that $GATA3^{WT}$ promotes the expression of many oncogenes, such as *MYB* and *ERα*, which enhance tumor growth potential and cause worse prognosis (33). Although GATA3 is considered to be play a critical role in breast cancer development, the role of GATA3 in breast cancer is still under debate (16). Here, we show that although aberrant GATA3 LLPS caused by its ZnF2 defective breast cancer-associated mutations significantly reduced the oncogenic potential of breast cancer, elevated expression of GATA3, whether mutated or not, plays an oncogenic role in breast cancer development. The ZnF-regulated LLPS of GATA3 provides a clinical phenotype-associated mechanism to unify explain the oncogenic role of GATA3 on the disease course of breast cancer, suggesting that LLPS of ZnF TFs regulated by their ZnFs may be useful for functional and mechanistic interpretation of disease-associated ZnF TF mutations in many malignant settings.

The immune system is essential for human health, and its dysfunction plays a central role in the development of various human diseases, including cancer (7). GATA3 is a master regulator in controlling the generation and function of immune cells, including various T cells, B cells, NK cells and ILC2 cells (9). The immune system is a highly sophisticated system that is a complex network of organs, immune cells, non-immune cells and proteins, where increasing studies have noticed essential roles of immune modulation by non-immune cells (18). For example, recently, we reported that breast cancer cells, as non-immune cells, facilitate the formation of an immune suppressive microenvironment by cancer-intrinsic BOMR-inhibited IRF3 (35). However, the function of GATA3 in regulating immunity in non-immune cells is largely unknown. Here, we show that aberrant GATA3 LLPS caused by its ZnF2 defective mutations promotes aberrant upregulation of immune gene expression and activation of type I IFN signaling in breast cancer cells, suggesting that ZnF2-regulated LLPS underlies the master role of GATA3 in immune regulation beyond immune cells. In cell nuclei, ZnF TFs are ubiquitously shown as microscopically visible chromatin condensates/speckles, known as CSCs, which are the direct localization of ZnF TFs in regulating their target gene expression (36). CSC formation and chromatin organization are ultimately associated with ZnF TFs in shaping the transcriptional network in human health cells and disease cells, including cancer cells for their oncogenic

behavior (33, 37, 38). The formation of CSCs is critical for the precisely regulated chromatin organization and gene transcription (39, 40). CSCs can contain many proteins, including TFs, mediators, histones and various chromatin proteins, and their formation can be modulated by various regulatory factors (41). HP1α and H3K9me3 are the two conserved hallmarks of heterochromatin (42). LLPS of HP1α is considered to be a driving mechanism underlying CSC formation and chromatin organization, where H3K9me3 generated by suv39H1 mediates LLPS of HP1α (43). LLPS is proposed to be one of the master mechanisms underlying ZnF TFs and CSC interactions, which are of fundamental importance for ZnF TFs in controlling the expression of genes critical for human health or disease (1, 44, 45). It's perhaps not surprising that Zn TFs have been implicated to be involved in LLPS-mediated CSC formation (36). However, the underlying mechanisms are only partially understood. Here, we found that aberrant GATA3 LLPS caused by ZnF2 defective mutations remarkably altered the chromatin organizations, but reduced suv39H1 and H3K9me3 levels through destabilizing suv39H1. Furthermore, suv39H1 inhibition by Chaetocin increased the GATA3-containing CSCs. Consistent with remarkably increased the expression of immune genes by GATA3 ZnF2 defective mutants compared to the wild-type protein, GATA3 ZnF2 defective mutants showed increased colocalization with transcription activation markers, including p300 and H3K27ac, supporting that the DBD of GATA3 and the ZnF2 in its DBD plays an important role in controlling gene expression through an LLPS-mediated mechanism. Interestingly, suv39H1 was recently found to be one of critical factors in regulating immunity, where inhibition suv39H1 activates TE-encoded retroviral antigens (ERVs) to induce TE-specific cytotoxic T cell responses and active innate immune against tumor (24, 46). Although chronic exposure to low levels of type I IFN provides important pro-survival advantages, hyperactivated type I IFN signaling drives growth arrest and apoptosis of cancer cells (47). Here, we found that in breast cancer cells, aberrant GATA3 LLPS caused by breast cancer-associated ZnF2 defective mutations results aberrant upregulation of type I IFN signaling-related immune genes and activation of type I IFN signaling. These results suggest that aberrant GATA3 LLPS caused by breast cancer-associated ZnF2 defective mutations hyperactivate type I IFN signaling to contribute to their reduced ability in promoting breast cancer growth.

In summary, our data demonstrate that ZnF2-regulated GATA3 LLPS underlies the role of GATA3 in breast cancer development and immune regulation. Since ZnFs are a common feature of the ZnF TF DBDs, by describing ZnF2-regulated GATA3 LLPS as a proof-of-principle, we asserted that the LLPS of ZnF TFs regulated by the ZnF in their DBDs is an important mechanism underlying the multifaceted function of ZnF TFs in human health and disease, such as cancer.

Materials and Methods

Plasmids.

The GATA3-mEGFP constructs were generated by PCR and subcloned into the pmEGFP-N2 mutated by pEGFP-N2 (Clontech). MBP-GATA3-mEGFP constructs were generated by PCR and subcloned into the pET-MBP-3C vector. Mutant GATA3-mEGFP containing various truncations and mutations in the GATA3 molecule were generated using PCR and similarly cloned into the above vectors. We initially designed primers to clone different regions of $GATA3^{WT}$ (443 amino acids), AD (1-260), DBD (261-360), C (361-443), △AD (261-443), △DBD (1-260+361-443) and △C (1-360). The $ZnF2^{de\text{-}X308}$ splice mutant is an example of a genome splice protein, which was generated by $GATA3^{WT}$. Other truncations of GATA3 were also generated by $GATA3^{WT}$, such as $ZnF2^{in\text{-}M293K}$, $ZnF2^{in\text{-}G360}$, $ZnF2^{de\text{-}R330}$, $ZnF1^{2R\text{-}A}$ (R275R276-A275A276), $ZnF2^{2R\text{-}A}$(R329R330-A329A330) and $GATA3^{4R\text{-}A}$ (R275R276R329R330-A275A276A329A330). Some constructs have mEGFP (monomeric EGFP, with A206K mutation of EGFP) fused at the C-terminus as indicated. Truncation mutants were generated by PCR cloning. The MBP-GATA3 plasmids were PCR by pmEGFP-N2-GATA3 variants to be inserted at the BamH I and Not I site in the pET-MBP-3C construct. HA-tag labeled GATA3 mutants and WT construct subclone to pCDH-CMV-MCS-EF1-copGFP-T2A-Puro, and BamH I and Nhe I site were used in pCDH-CMV-MCS-EF1-copGFP-T2A-Puro. The primers were listed in *SI Appendix*, Table S1.

Cell culture, transfection, infection.

Cells were maintained accordingly to the guidance from American Type Culture Collection. Human HEK293T were cultured in DMEM supplemented with 10% (v/v) FBS, 100 units/mL penicillin and 100 mg/mL streptomycin. MCF7,4T1were cultured in RPMI1640 supplemented with 10% (v/v) FBS, 100 units/mL penicillin and 100 mg/mL streptomycin. All cells were cultured at 37 ℃ in a humidified atmosphere of 95% air and 5% CO2. HEK293T, T47D, MCF7, and 4T1 cells have been verified through periodic morphology checks and mycoplasma detection. Transfection of cells was performed using Lipo2000 (Thermo Fisher Scientific) according to the manufacturer's instructions. After transfection to cells, incubation 24h and imaged using the confocal system. In IF assay, all of GATA3 and GATA3 variants were transient transfection into the HEK293T, MCF7 and T47D cells. The stable GATA3 cells expressing GATA3 variants were generated by retroviral infection for GATA3 and 4T1 cells, using pCDH-CMV-MCS-EF1-copGFP-T2A-Puro. Briefly, HA-tag labeled GATA3 mutants and WT construct subclone to pCDH-CMV, then transfection to HEK293T cells 48h. Collection virus to infection cells, after 48h incubation, 2ug/ml puromycin was used to choosing stable expression GATA3 WT and mutants cells 14 days.

Generation of MCF7$^{GATA3\text{-}KO}$ cell line.

Briefly, the guide RNA was designed by the Dr.Feng Zhang Laboratory webtool(crispr.mit.edu). The double-stranded oligonucleotides were inserted into the lentiCRISPR-v2(Addgene plasmid 52961). The primers were listed in *SI Appendix*, Table S2. HEK293T cells were co-transfected with the 2 μg lentiCRISPR-v2 vector and lentivirus packaging plasmid1.5 μg pSPAX2 and 0.5 μg pMD2. G, plasmid using Lipofectamine 2000 reagent according to the manufacturer's instructions. After incubation 48h, collection virus to infection MCF7 cells, after 48h incubation, 2ug/ml puromycin was used to choosing positive cells. Then positive cells limit dilution were spread into 96-well plates to culture. After 2 weeks, see significate colon in 96-well plates, and choosing these cells to detect GATA3 using western blot.

High content image.

HEK293T cells expressing GATA3^{WT}, GATA3 truncations (N, C, DBD, △N, △C and △DBD) and GATA3 mutants (ZnF2$^{in\text{-}2R\text{-}A}$, ZnF2$^{de\text{-}2R\text{-}A}$, and GATA3$^{de\text{-}4R\text{-}A}$)–mEGFP were seeded in 24-well glass bottom plate (Sofa P24-1.5H-N) and images were obtained with the NIS-element cell imaging analysis system (Nico TIAR). The100x objective lens was applied in each condition. Data was analyzed by images collected from 10 representative fields in each group. Single cells were identified based on DAPI as reference, while the spots quantification was performed based on the area and intensity of the spots through mEGFP channel. MCF7$^{GATA3\text{-}KO}$ or T47D cells expressing GATA3^{WT} and GATA3 mutants (ZnF2^{in} mutants, ZnF2^{de} mutants) and images were obtained with the NIS-element cell imaging analysis system (Nico TIAR). Endogenous p300, H3K27ac and H3K9me3 with binding to Alexa 594 was also detected with mEGFP-tag GATA3 in MCF7$^{GATA3\text{-}KO}$ cells. The original images resolution is 1024 x 1024 pixel^2. In set means zoom at 3X set.

Fluorescence Recovery After Photobleaching (FRAP).

FRAP assay was conducted using the FRAP module of the Zeiss LSM710/810 ZEN blue confocal microscopy system. The GATA3-mEGFP proteins were bleached using a 488nm laser beam. Bleaching was focused on a circular region of interest (1-2μm) using 100% laser power, after about 5 seconds, time-lapse (2 seconds per image) images were collected. For GATA3 droplets in live-cell, Leica STELLARIS STED or Zeiss LSM710 for use to assay. Zeiss LSM710 bleaching set is consisting of protein in vitro and in vivo. For Stellaris STED, bleaching time is 3 seconds, and the time interval is 2 seconds per image. Time images remain 10 min. Fluorescence intensity was measured using the ZEN blue or Leica system. Background intensity was subtracted and values are reported relative to pre-bleaching time points. Percent recovery for each time point was calculated as $(I - I_{min})/ (I_0 - I_{min}) \times 100\%$, in which I, I_{min}, and I_0 are the normalized intensity for each time point, minimum (0 s after bleaching), and initial (before bleaching) intensities, respectively. FRAP recovery curves were fitted to generate half time of recovery for each bleached condensate, which was used to calculate the mean and s.d. of the half time. Graph Pad Prism is used to plot and analyze the FRAP results.

Immunofluorescence staining and live-cell imaging.

Immunofluorescence was performed following standard protocols. Brefily, cells were washed with PBS and fixed with ice-cold methanol for 15 min, then cells were cultured at Triton-100 for 30

min. Cells were incubated with rabbit antibody p300(abcam, ab275378,1:200), H3K27ac (abcam, ab4729,1:200) and H3K9me3(abcam, ab8898:1:200) at 4℃ overnight, then incubated with Alexa flour 594 goat anti-rabbit antibody (abcam, ab150080,1:200) for 2 hours at room temperature. The slides were further counterstained with DAPI. For live-cell imaging, cells were cultured in 35□mm glass-bottom dishes (Corning), and used for imaging on a Zeiss LSM710 confocal microscope supported with a Chamlide TC temperature, humidity, and CO_2 chamber.

Protein expression and purification.

Plasmids containing mEGFP-His or MBP-tagged genes were transformed into E. coli BL21 cells. All proteins were expressed in Escherichia coli BL21 (DE3)-Rosetta cells. Cells were grown to OD 0.6-0.8 at 37℃ in LB media with 100 mg/ml Ampicillin. E. coli cells expressing protein were induced with 0.1-0.3mM IPTG at 16℃ for 18 hours, and Sonication in lysis buffer (50 mM Tris-HCl pH 7.5, 500 mM NaCl, 1 mM PMSF). Cells were at 80% of 300 W power, on 5 s, off 10 s, remains buffer clarify. These proteins were first purified using Ni affinity chromatography, and then further purified using Superdex 200 Increase 10/300 GL. These proteins were flash frozen in liquid nitrogen, then stored in 50 mM Tris-HCl pH 7.5, 500 mM NaCl, 1 mM DTT, 10% glycerol at -80℃. Purified proteins were examined by SDS–PAGE followed by Coomassie blue staining. Protein concentration was determined by Nanodrop measurement for OD 562 and calculation using extinction coefficient provided by ExPASy ProtParam (https://web. expasy.org/protparam/), and validated by comparison with Coomassie blue staining of known concentrations of BSA.

In vitro droplets formation and turbidity assays.

In vitro LLPS experiments were performed at room temperature unless otherwise indicated. For the droplet formation assay, the purified $GATA3^{WT}$ or GATA3 mutant proteins without mEGFP-tag were mixed with a buffer containing 50 mM Tris pH 7.4 and incubated for 2 hours at room temperature after adding proteinase 3C in different NaCl concentration. Samples were observed under a DIC microscope using a Leica DMi8 microscope with a 40x objective. PreScission protease 3C cleavage MBP-tag for recombinant protein N terminal. MBP-mEGFP and MBP-GATA3 variants mEGFP also performed at room temperature with a buffer containing 50 mM Tris pH 7.4 and incubated for 2 hours at room temperature after adding proteinase 3C in different NaCl concentration. Finally, 10μL of each sample was pipetted onto a glass dish and imaged using a Nico TIAR microscope. Under the same conditions, 10 μL of each sample was added to 384-well white polystyrene plate with a clear flat bottom, and the value of OD600 was measured by using a TECAN Infinite F PLEX Pro microplate reader (37℃, 2hr). For protein and DNA mixing, special GATA-DNA or no-GATA-DNA was incubation before GATA3 proteins under PreScission protease 3C cleaving, then 10 μL of each sample was added to 384-well white polystyrene plate with a clear flat bottom and images. The DNA-sequence as description were listed in *SI Appendix*, Table S3.

RNA extraction, reverse transcription and qPCR.

Total RNA was extracted using XGEN Reagent. RNA (1μg) was reverse-transcribed using the SuperScript III First-Strand Synthesis System (Vazyme). All experiments were carried out by following the manufacturers' instructions. In brief, RNAs were reverse-transcribed into cDNA using HiScript II Q-RT Super Mix (Vazyme), and qPCR was performed using ChamQ SYBR Q-PCR Master Mix (Vazyme). The relative expression levels of mRNAs and mRNAs were calculated according to the $2^{-\Delta\Delta Ct}$ method. GAPDH served as the internal control. Primer sequences for RT–qPCR are listed in *SI Appendix*, Table S4.

Western blot.

Cells were lysed in RIPA lysis buffer (Beyotime, P10030B) supplemented with 1 mM 1 mM phenylmethylsulfonyl fluoride (PMSF). Protein concentrations were quantified with the BSA protein assay kit. Western blotting was performed as previously described(48). Briefly, 30 μg of protein extracts were loaded and separated by SDS-PAGE gels. Blotting was performed using standard protocols. All of 0.45μm and 0.22 μm PVDF membranes (Millipore) were used. Membranes were blocked for 1 hour in blocking buffer (5% BSA in TBST) followed by primary

antibody probes at 4°C. Membranes were incubated with HRP-conjugated secondary antibodies after three washes with PBST. Signals were detected using BeyoECL Plus (Beyotime, P0018S). All antibodies used for immunoblotting are listed in *SI Appendix*, Table S5.

RNA library constructing and sequencing

1 μg total RNA was used for following library preparation. The poly(A) mRNA isolation was performed using Oligo(dT) beads. The mRNA fragmentation was performed using divalent cations and high temperature. Priming was performed using Random Primers. First strand cDNA and the second-strand cDNA were synthesized. The purified double-stranded cDNA was then treated to repair both ends and add a dA-tailing in one reaction, followed by a T-A ligation to add adaptors to both ends. Size selection of Adaptor-ligated DNA was then performed using DNA Clean Beads. Each sample was then amplified by PCR using P5 and P7 primers and the PCR products were validated. Then libraries with different indexs were multiplexed and loaded on an Illumina HiSeq/ Illumina Novaseq/MGI2000 instrument for sequencing using a 2x150 paired-end (PE) configuration according to manufacturer's instructions. Differential expression analysis used the DESeq2 Bioconductor package, a model based on the negative binomial distribution. the estimates of dispersion and logarithmic fold changes incorporate data-driven prior distributions.For volcano plots, log2FC>1 or<-1, p<0.05 were used to screening differential gene expression and Sanger box tool (http://sangerbox.com/) was used to draw volcano plots. For GSEA analysis, WebGestalt (WEB-based GEne SeT AnaLysis Toolkit) was used .

Cell growth assay.

For cell growth, GATA3 variants stable expressing MCF7 cells were seeded in a 12-well plate for $1*10^5$ and counted the number of cells number (1,2,3,4 day). Graph Pad Prism is used to plot and analyze the results.

Tumor assays in mice.

Mice were housed in AAALAC-accredited facilities and maintained on a 12□h light:12□h dark-light cycle with room temperatures of 21–23□°C with 40–60% humidity. Mice were housed separated by sex (n□=□5 per cage) in corncob bedding with filter-top lids. The maximal tumor measurement permitted by IACUC is 20□mm the largest diameter. Tumor volumes and other endpoints did not exceed the limits permitted by IACUC. All mice were maintained under specific pathogen-free conditions and housed in individually ventilated cages.

4T1 cells transduced with the GATA3 constructs were resuspended in 100□μl PBS and injected into the tail vein of 7-week-old BALB/C mice. Tumor size was measured on the two longest dimensions using a Vernier caliper. Tumor volume (V) was calculated with the formula $V = D_1(D_2)^2/2$, where D_1 is the long dimension and D_2 is the short dimension. Twenty days after transplantation, mice were humanely euthanized to collect tumors.

Materials Availability.

Plasmids, compounds, and cell lines generated in this study will be made available upon request. We may require a payment and/or a completed Materials Transfer Agreement in case there is potential for commercial application

Statistics and reproducibility.

All data are expressed as mean ± s.d. and analyzed using GraphPad Prism 7.0 software. For experiments consisting of only two groups, the data were evaluated by Student's t-test (two tails). For experiments involving multiple groups, the data were analyzed by one-way analysis of variance. For survival analysis, log rank p was used. When $p < 0.05$, statistical analysis considers statistical significance.

Data Availability.

Additional procedures are described in SI Appendix, Supplementary Information Text. All study data are included in the article and SI Appendix.

Acknowledgments

This work was supported by the National Natural Science Foundation of China (81974447), Natural Science Foundation of Jiangsu Province (SBK2020010058), and the Priority Academic Program Development of Jiangsu Higher Education Institutions.

References

1. J. Jen, Y. C. Wang, Zinc finger proteins in cancer progression. *J Biomed Sci* **23**, 53 (2016).
2. M. Cassandri *et al.*, Zinc-finger proteins in health and disease. *Cell Death Discov* **3**, 17071 (2017).
3. B. Wang *et al.*, Liquid-liquid phase separation in human health and diseases. *Signal Transduction and Targeted Therapy* **6** (2021).
4. W. Borcherds, A. Bremer, M. B. Borgia, T. Mittag, How do intrinsically disordered protein regions encode a driving force for liquid-liquid phase separation? *Curr Opin Struc Biol* **67**, 41-50 (2021).
5. A. Boija *et al.*, Transcription Factors Activate Genes through the Phase-Separation Capacity of Their Activation Domains. *Cell* **175**, 1842-+ (2018).
6. M. H. Lentjes *et al.*, The emerging role of GATA transcription factors in development and disease. *Expert Rev Mol Med* **18**, e3 (2016).
7. H. Ikeda, Y. Togashi, Aging, cancer, and antitumor immunity. *Int J Clin Oncol* **27**, 316-322 (2022).
8. M. J. Ellis *et al.*, Whole-genome analysis informs breast cancer response to aromatase inhibition. *Nature* **486**, 353-360 (2012).
9. Y. Y. Wan, GATA3: a master of many trades in immune regulation. *Trends Immunol* **35**, 233-242 (2014).
10. T. C. Voss, G. L. Hager, Dynamic regulation of transcriptional states by chromatin and transcription factors. *Nat Rev Genet* **15**, 69-81 (2014).
11. K. Rippe, Liquid-Liquid Phase Separation in Chromatin. *Csh Perspect Biol* **14** (2022).
12. S. K. Rai, R. Khanna, A. Avni, S. Mukhopadhyay, Heterotypic electrostatic interactions control complex phase separation of tau and prion into multiphasic condensates and co-aggregates. *Proceedings of the National Academy of Sciences* **120**, e2216338120 (2023).
13. J. Yang *et al.*, Electrostatic interactions in molecular recognition of intrinsically disordered proteins. *J Biomol Struct Dyn* **38**, 4883-4894 (2020).
14. Y. Chen *et al.*, DNA binding by GATA transcription factor suggests mechanisms of DNA looping and long-range gene regulation. *Cell Rep* **2**, 1197-1206 (2012).
15. R. Kumar *et al.*, Structural and conformational changes induced by missense variants in the zinc finger domains of GATA3 involved in breast cancer. *RSC Adv* **10**, 39640-39653 (2020).
16. M. Takaku, S. A. Grimm, P. A. Wade, GATA3 in Breast Cancer: Tumor Suppressor or Oncogene? *Gene Expr* **16**, 163-168 (2015).
17. R. Asch-Kendrick, A. Cimino-Mathews, The role of GATA3 in breast carcinomas: a review. *Hum Pathol* **48**, 37-47 (2016).
18. T. Dainichi, K. Kabashima, Ivanov, II, Y. Goto, Editorial: Regulation of Immunity by Non-Immune Cells. *Front Immunol* **12**, 770847 (2021).
19. S. Liu *et al.*, Phosphorylation of innate immune adaptor proteins MAVS, STING, and TRIF induces IRF3 activation. *Science* **347**, aaa2630 (2015).
20. J. Loven *et al.*, Selective inhibition of tumor oncogenes by disruption of super-enhancers. *Cell* **153**, 320-334 (2013).
21. E. Ortega *et al.*, Transcription factor dimerization activates the p300 acetyltransferase. *Nature* **562**, 538-544 (2018).
22. E. J. Richards, S. C. Elgin, Epigenetic codes for heterochromatin formation and silencing: rounding up the usual suspects. *Cell* **108**, 489-500 (2002).

23. S. Sanulli *et al.*, HP1 reshapes nucleosome core to promote phase separation of heterochromatin. *Nature* **575**, 390-394 (2019).
24. J. Padeken, S. P. Methot, S. M. Gasser, Establishment of H3K9-methylated heterochromatin and its functions in tissue differentiation and maintenance. *Nature Reviews Molecular Cell Biology* **23**, 623-640 (2022).
25. A. Kanhere *et al.*, T-bet and GATA3 orchestrate Th1 and Th2 differentiation through lineage-specific targeting of distal regulatory elements. *Nature Communications* **3** (2012).
26. A. Kanhere *et al.*, T-bet and GATA3 orchestrate Th1 and Th2 differentiation through lineage-specific targeting of distal regulatory elements. *Nat Commun* **3**, 1268 (2012).
27. J. H. Ahn *et al.*, Phase separation drives aberrant chromatin looping and cancer development. *Nature* **595**, 591-595 (2021).
28. S. Alberti, Phase separation in biology. *Curr Biol* **27**, R1097-R1102 (2017).
29. J. J. Bouchard *et al.*, Cancer Mutations of the Tumor Suppressor SPOP Disrupt the Formation of Active, Phase-Separated Compartments. *Mol Cell* **72**, 19-36 e18 (2018).
30. S. J. Nair *et al.*, Phase separation of ligand-activated enhancers licenses cooperative chromosomal enhancer assembly. *Nat Struct Mol Biol* **26**, 193-203 (2019).
31. H. Sung *et al.*, Global Cancer Statistics 2020: GLOBOCAN Estimates of Incidence and Mortality Worldwide for 36 Cancers in 185 Countries. *CA Cancer J Clin* **71**, 209-249 (2021).
32. B. Nogrady, How cancer genomics is transforming diagnosis and treatment. *Nature* **579**, S10-S11 (2020).
33. N. Hruschka *et al.*, The GATA3 X308_Splice breast cancer mutation is a hormone context-dependent oncogenic driver. *Oncogene* **39**, 5455-5467 (2020).
34. M. Takaku *et al.*, GATA3 zinc finger 2 mutations reprogram the breast cancer transcriptional network. *Nat Commun* **9**, 1059 (2018).
35. W. Liu *et al.*, A brain-enriched lncRNA shields cancer cells from immune-mediated killing for metastatic colonization in the brain. *Proc Natl Acad Sci U S A* **119**, e2200230119 (2022).
36. R. Sharma *et al.*, Liquid condensation of reprogramming factor KLF4 with DNA provides a mechanism for chromatin organization. *Nat Commun* **12**, 5579 (2021).
37. K. M. A. Dreijerink *et al.*, Enhancer-Mediated Oncogenic Function of the Menin Tumor Suppressor in Breast Cancer. *Cell Rep* **18**, 2359-2372 (2017).
38. Y. Shin *et al.*, Liquid Nuclear Condensates Mechanically Sense and Restructure the Genome. *Cell* **175**, 1481-1491 e1413 (2018).
39. J. C. Hansen, K. Maeshima, M. J. Hendzel, The solid and liquid states of chromatin. *Epigenetics Chromatin* **14**, 50 (2021).
40. G. J. Narlikar, Phase-separation in chromatin organization. *Journal of Biosciences* **45** (2020).
41. B. A. Gibson *et al.*, Organization of Chromatin by Intrinsic and Regulated Phase Separation. *Cell* **179**, 470-484 e421 (2019).
42. C.-W. Chang, Y.-C. Shen, S.-J. Yan, HP1a-mediated heterochromatin formation inhibits high dietary sugar-induced tumor progression. *Cell Death & Disease* **12**, 1130 (2021).
43. L. Wang *et al.*, Histone Modifications Regulate Chromatin Compartmentalization by Contributing to a Phase Separation Mechanism. *Mol Cell* **76**, 646-659.e646 (2019).

44. F. D. Urnov, A feel for the template: zinc finger protein transcription factors and chromatin. *Biochem Cell Biol* **80**, 321-333 (2002).
45. R. Karn, I. A. Emerson, Breast cancer mutation in GATA3 zinc finger 1 induces conformational changes leading to the closer binding of ZnFn2 with a wrapping architecture. *J Biomol Struct Dyn* **38**, 1810-1821 (2020).
46. D. Pan *et al.*, SETDB1 Restrains Endogenous Retrovirus Expression and Antitumor Immunity during Radiotherapy. *Cancer Res* **82**, 2748-2760 (2022).
47. H. Cheon, Y. Wang, S. M. Wightman, M. W. Jackson, G. R. Stark, How cancer cells make and respond to interferon-I. *Trends Cancer* **9**, 83-92 (2023).
48. Z. Liu *et al.*, Enhancer activation requires trans-recruitment of a mega transcription factor complex. *Cell* **159**, 358-373 (2014).

Figure legends

Fig. 1. GATA3 undergoes LLPS in cells and in vitro. (*A*) Representative confocal microscopy images of HEK293T cells with ectopic overexpression of mEGFP-tagged wild type GATA3 ($GATA3^{WT}$). Scale bar, 5 μm. (*B*) Representative confocal microscopy images of Hela cells with ectopic overexpression of mEGFP-tagged $GATA3^{WT}$. Scale bar, 2 μm. (*C*) Representative confocal microscopy images of HEK293T cells with ectopic overexpression of mEGFP-tagged $GATA3^{WT}$ after treatment with 10% 1,6-hexanediol (1.6-Hex) compared to control. Scale bar,2 μm. (*D*) Representative images of mEGFP-tagged $GATA3^{WT}$ droplets in HEK293T cells across time in FRAP assay. Scale bar, 2 μm. (*E*) Normalized fluorescence recovery of mEGFP-tagged $GATA3^{WT}$ droplets in HEK293T cells as shown in (*D*), $t_{1/2}$, means half-life of recovery time. (*F*) Representative images of 10 μM purified MBP-$GATA3^{WT}$ protein without mEGFP tag in tubes treated with 3C protease treatment compared to control. (*G*) Representative images of droplets formed by 10 μM purified MBP-$GATA3^{WT}$ protein without mEGFP tag with 3C protease treatment compared to control. Scale bar, 50 μm. (*H*) Representative images of droplets formed by 10 μM purified MBP-$GATA3^{WT}$ protein with mEGFP tag compared to 10 μM purified MBP-mEGFP protein post the MBP cleaved by 3C protease treatment. Scale bar, 10 μm. (*I*) FRAP assay for droplets formed by 10 μM purified MBP-$GATA3^{WT}$ protein with mEGFP tag after its MBP was cleaved by 3C protease treatment. Right, representative images of droplets across time in the FRAP assay. Light, normalized fluorescence recovery of droplets in FRAP assay. Scale bar, 1μm. (*J*) Representative images of droplet fusion events using 10 μM purified MBP-$GATA3^{WT}$ protein with mEGFP tag after its MBP was cleaved by 3C protease treatment. Scale bar, 5 μm.

Fig. 2. The DBD of GATA3 regulate phase separation via MEIs. (*A*) Disordered tendency analysis of GATA3 protein sequences. Top, A diagram shows the domain organization of GATA3. Bottom, PONDR assigned scores to the GATA3 protein sequence. A score higher than 0.5 indicates disordered regions (Green), and lower than 0.5 indicates ordered regions (Purple). (*B*) Representative confocal microscopy images of HEK293T cells with ectopic overexpression of mEGFP-tagged $GATA3^{WT}$ and mEGFP-tagged truncations. Scale bar, 2 μm. (*C*) Quantification of the number of droplets per cell shown in (*B*). Biologically independent samples in triplicate: 20-50 transfected cells in each sample were quantified. Data are mean□±□s.d.. *, $p<0.05$; **, $p<0.01$; ***, $p<0.001$ (t-test), ns, not significant. (*D*) Representative images of droplets formed by 10 μM purified different MBP-GATA3 domain truncated proteins without mEGFP tag compared to 10 μM purified MBP-$GATA3^{WT}$ protein without mEGFP tag after cleavage of MBP by 3C protease treatment. Scale bar, 20 μm. (*E*) Average charge analysis of the GATA3 protein amino acid sequence. Red, negatively charged; blue, positively charged. Orange, DBD region. (*F*) Representative images of droplets formed by 5 μM GATA3-mEGFP with increasing NaCl concentration from 37.5 mM to 300 mM as indicated in the figure. Scale bar, 10 μm. (*G*) Quantification of the percentage of areas covered by droplets in the visual fields. Data are mean□±□s.d.. *, $p<0.05$; **, $p<0.01$; ***, $p<0.001$(t-test). (*H*) Diagrams summarizing the LLPS of $GATA3^{WT}$ and GATA3 domain truncated proteins with increasing of protein concentration from

0.25 μM to 10 μM along with increasing of NaCl concentration from 37.5mM to 500 mM as indicated in the figures. Green dots, LLPS; red dots, no LLPS.

Fig. 3. ZnF2 and its amino acids R329 and R330 regulate the LLPS of GATA3. (*A*) A representative image elucidating the complex structure of ZnF1 in GATA3 binding to DNA (PDB: 4HC9). (*B*) A representative image elucidating the complex structure of ZnF2 in GATA3 binding to DNA (PDB: 4HC7). (*C*) Representative confocal microscopy images of HEK293T cells with ectopic overexpression of mEGFP-tagged GATA3 mutants compared to mEGFP-tagged $GATA3^{WT}$ as indicated in the figure. Scale bar, 2 μm. (*D*) Quantification of the number of droplets per cell shown in (*C*). Data are mean±s.d.. ***, p<0.001; ns, not significant (t-test). (*E*) Representative images of droplets formed by 10 μM purified MBP- $ZnF2^{2R-A}$ protein with mEGFP tag after the MBP cleaved by 3C protease treatment. Scale bar, 10 μm. (*F*) Representative images of mEGFP-tagged $ZnF2^{2R-A}$ droplets compared to mEGFP-tagged $GATA3^{WT}$ droplets in HEK293T cells across time in FRAP assay. Scale bars, 2 μm. (*G*) Normalized fluorescence recovery of mEGFP-tagged $ZnF2^{2R-A}$(Red) droplets compared to mEGFP-tagged $GATA3^{WT}$ (Blue) droplets in HEK293T cells as shown in (*D*), $t_{1/2}$, half-life of recovery time. (*H*) Quantification the size of droplets formed by 10 μM purified MBP- $GATA3^{WT}$ protein with mEGFP tag and the MBP cleaved by 3C protease treatment in the visual fields, and DNA treatment was indicated in the figure. Blue, noGATA-DNA added. Red, GATA-DNA added. Black, no DNA added. GATA3-mEGFP protein concentration, 10 μM. (*I*) Representative images of droplets formed by 10 μM purified MBP- $GATA3^{WT}$ protein with mEGFP tag and the MBP cleaved by 3C protease treatment with 20 μM noGATA-DNA or 20 μM GATA-DNA added compared to no DNA added. (*J*) Representative images of droplets formed by 10 μM purified mEGFP-tagged $ZnF2^{2R-A}$ protein compared to 10 μM purified mEGFP-tagged $GATA3^{WT}$ protein with 20 μM noGATA-DNA or 20 μM GATA-DNA added as indicated in the figure across time in FRAP assay. The MBP of purified proteins was cleaved by 3C protease treatment. Scale bars, 10 μm. (*K*) Normalized fluorescence recovery of droplets as shown in (*D*). Blue, 20 μM no-GATA DNA added. Red, 20 μM GATA DNA added. Black, no DNA added.

Fig. 4. ZnF2-regulated LLPS of GATA3 unify explain the oncogenic role of GATA3 in breast cancer development. (*A*) A diagram summarizing the GATA3 mutations identified in clinical breast cancer samples. Black dots, GATA3 truncating mutations. Yellow dots, GATA3 inframe mutations. Red dots, GATA3 missense mutations. (*B*) Representative confocal microscopy images of HEK293T cells with ectopic overexpression of mEGFP-tagged breast cancer-associated GATA3 mutants compared to mEGFP-tagged $GATA3^{WT}$ as indicated in the figure. Scale bar, 5μm. (*C*) Quantification of the number of droplets per cell shown in (*B*). Data are mean ± s.d.. ***, p<0.001 (t-test). (*D*) Images of HEK293T cells with ectopic expression of $GATA3^{de-X308}$ genes and treatment with 10% 1,6-heleax indicated 1min. Scale bar, 2μm. (*E*) Representative confocal microscopy images of breast cancer T47D and $MCF7^{GATA3-KO}$ cells with with ectopic overexpression of mEGFP-tagged breast cancer-associated GATA3 mutants compared to mEGFP-tagged $GATA3^{WT}$ as indicated in the figure. $MCF7^{GATA3-KO}$ is MCF7 with both endogenous $GATA3^{WT}$ and $GATA3^{mu}$ knocked out by Cas9. Scale bar, 5μm. (*F*) Overall survival analysis of breast cancer patients with different types of mutations compared to those with wild type GATA3. $GATA3^{WT}$(n=903): wild-type GATA3, $ZnF2^{de}$(n=92): GATA3 mutations with defective ZnF2, $ZnF2^{in}$(n=86): GATA3 mutations with intact ZnF2. **, p<0.01; ***, p<0.001 (log-rank p). (*G*) Growth potential of $MCF7^{GATA3-KO}$ cells with ectopic overexpression expression of indicated GATA3 wild type or mutated genes *in vitro* by proliferation assay. Data are mean ± s.d.. ***, p < 0.001 (t-test). (*H*) Growth potential of 4T1 cells with ectopic overexpression expression of indicated GATA3 wild type or mutated genes *in vivo* using xenograft breast cancer mouse model. Scale bar, 1cm. (*I*) Quantification of tumor volumes in (*H*). Data are mean ± s.d.. *, p < 0.05; **, p < 0.01 (t-test).

Fig. 5. ZnF2-regulated LLPS of GATA3 underlies its master immune regulatory function beyond immune cells. (*A*) Volcano plots representing the expression changes of all genes: significantly down- and up-regulated genes ($GATA3^{WT}$ VS $ZnF2^{2R-A}$, $GATA3^{WT}$ VS $ZnF2^{de-X308}$, $GATA3^{WT}$ VS $ZnF2^{de-R330}$: |log2 FC| >1 and p < 0.05) are colored blue and red, respectively; genes that do not show significant expression changes are colored gray; selected differentially expressed immune

genes are labeled with gene names. (*B*) A heatmap depicting the common differently altered genes in ZnF2 defective mutants including $ZnF2^{2R\text{-}A}$, $ZnF2^{de\text{-}X308}$, and $ZnF2^{de\text{-}R330}$ compared to $GATA3^{WT}$, where upregulated genes are colored red, downregulated genes are colored blue, and "*" marks ISGs. (*C*) *ISG15*, *IFI6*, *IFI27*, *IFI44*, *IFIT1* and *IFITM1* expression in $MCF7^{GATA3\text{-}KO}$ with ectopic overexpression expression of $ZnF2^{2R\text{-}A}$, $ZnF2^{de\text{-}X308}$, and $ZnF2^{de\text{-}R330}$ compared to $GATA3^{WT}$ by RT-qPCR. Data are mean ± s.d.. **, $p < 0.01$; ***, $p < 0.001$ (t-test). (*E*) Representative images of western blot analysis showing the level of IRF3, p-IRF3-S389/S396, TBK1 and p-TBK1-S172 in $MCF7^{GATA3\text{-}KO}$ with ectopic overexpression of $ZnF2^{2R\text{-}A}$, $ZnF2^{de\text{-}X308}$, and $ZnF2^{de\text{-}R330}$ compared to $GATA3^{WT}$. GAPDH was used as an internal loading control. (*F-H*) Representative immunofluorescence confocal microscopy images by using different chromatin markers as indicated in the figures in $MCF7^{GATA3\text{-}KO}$ with ectopic overexpression expression of $ZnF2^{2R\text{-}A}$ and $ZnF2^{de\text{-}X308}$ compared to $GATA3^{WT}$. Green: $GATA3^{WT}$, $ZnF2^{2R\text{-}A}$, or $ZnF2^{de\text{-}X308}$. Red: chromatin markers, including p300 (F), H3K27ac (G) and H3K9me3 (H). Blue: DAPI. Scale bar,2μm. (*I*) Representative images of western blot analysis showing the level of suv39H1, SETDB1 and H3K9me3 in $MCF7^{GATA3\text{-}KO}$ with ectopic overexpression of $ZnF2^{2R\text{-}A}$, $ZnF2^{de\text{-}X308}$, and $ZnF2^{de\text{-}R330}$ compared to $GATA3^{WT}$. (*J*) The impacts of suv39H1 inhibitor-Chaetocin treatment. Above, Representative immunofluorescence confocal microscopy images showing the impact of Chaetocin treatment on GATA3 condensation on chromatin in $MCF7^{GATA3\text{-}KO}$ with ectopic overexpression expression of $GATA3^{WT}$ compared to control. Chaetocin,100 nM. Control: DMSO. Scale bar, 2 μm. Below, the impact of Chaetocin treatment on the expression of GATA3-bound ISGs as indicated in the figure in $MCF7^{GATA3\text{-}KO}$ with ectopic overexpression expression of $GATA3^{WT}$ by RT-qPCR. Data are mean ± s.d.. **, $p < 0.01$; ***, $p < 0.001$ (t-test).

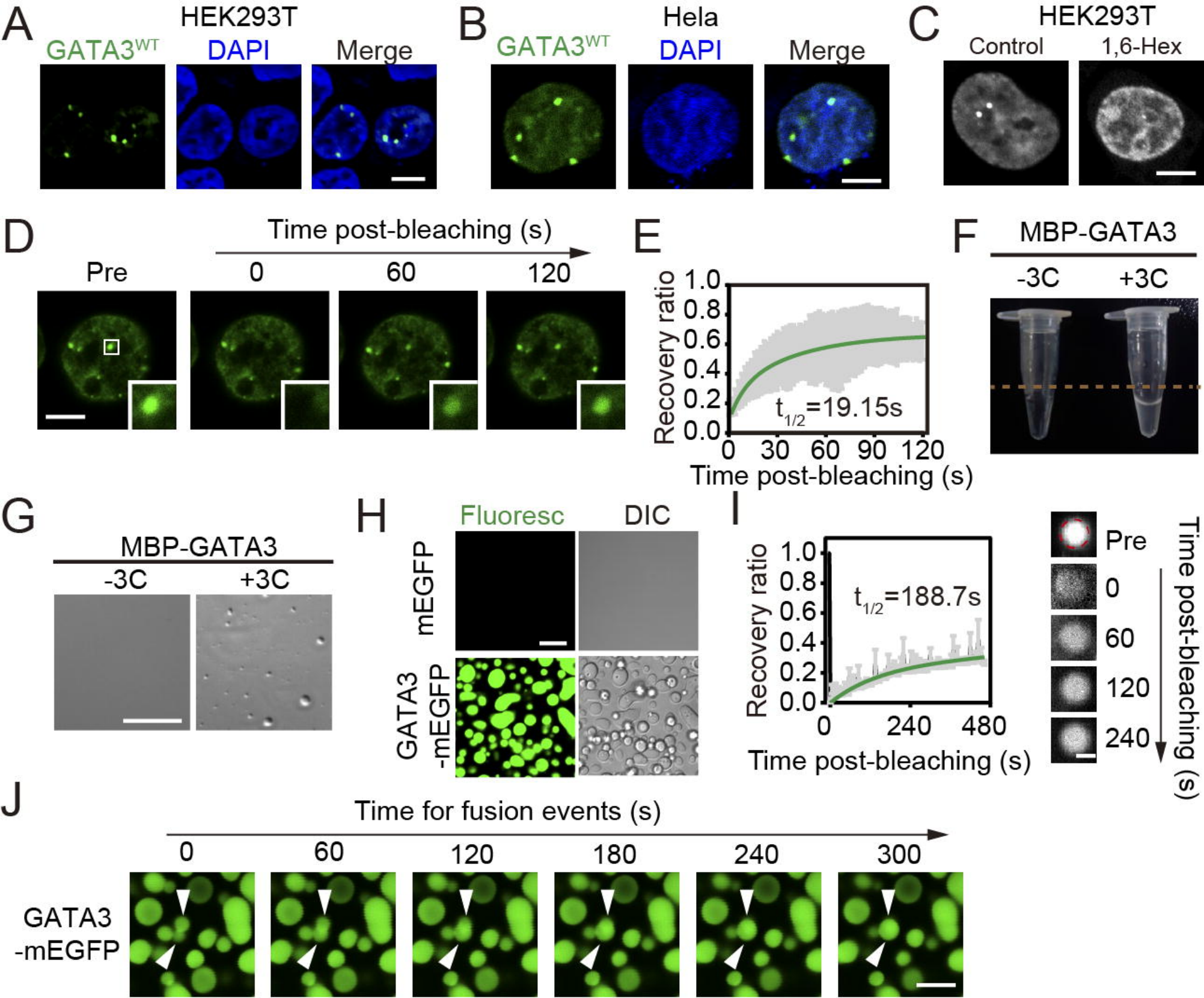
A
HEK293T
GATA3WT
DAPI
Merge
B
Hela
GATA3WT
DAPI
Merge
C
HEK293T
Control
1,6-Hex
D
Time post-bleaching (s)
Pre
0
60
120
E
Recovery ratio
1.0
0.8
0.6
0.4
0.2
0.0
t1/2=19.15s
0
30
60
90
120
Time post-bleaching (s)
F
MBP-GATA3
-3C
+3C
G
MBP-GATA3
-3C
+3C
H
Fluoresc
DIC
mEGFP
GATA3
-mEGFP
I
Recovery ratio
1.0
0.8
0.6
0.4
0.2
0.0
t1/2=188.7s
0
240
480
Time post-bleaching (s)
Pre
0
60
120
240
Time post-bleaching (s)
J
Time for fusion events (s)
0
60
120
180
240
300
GATA3
-mEGFP

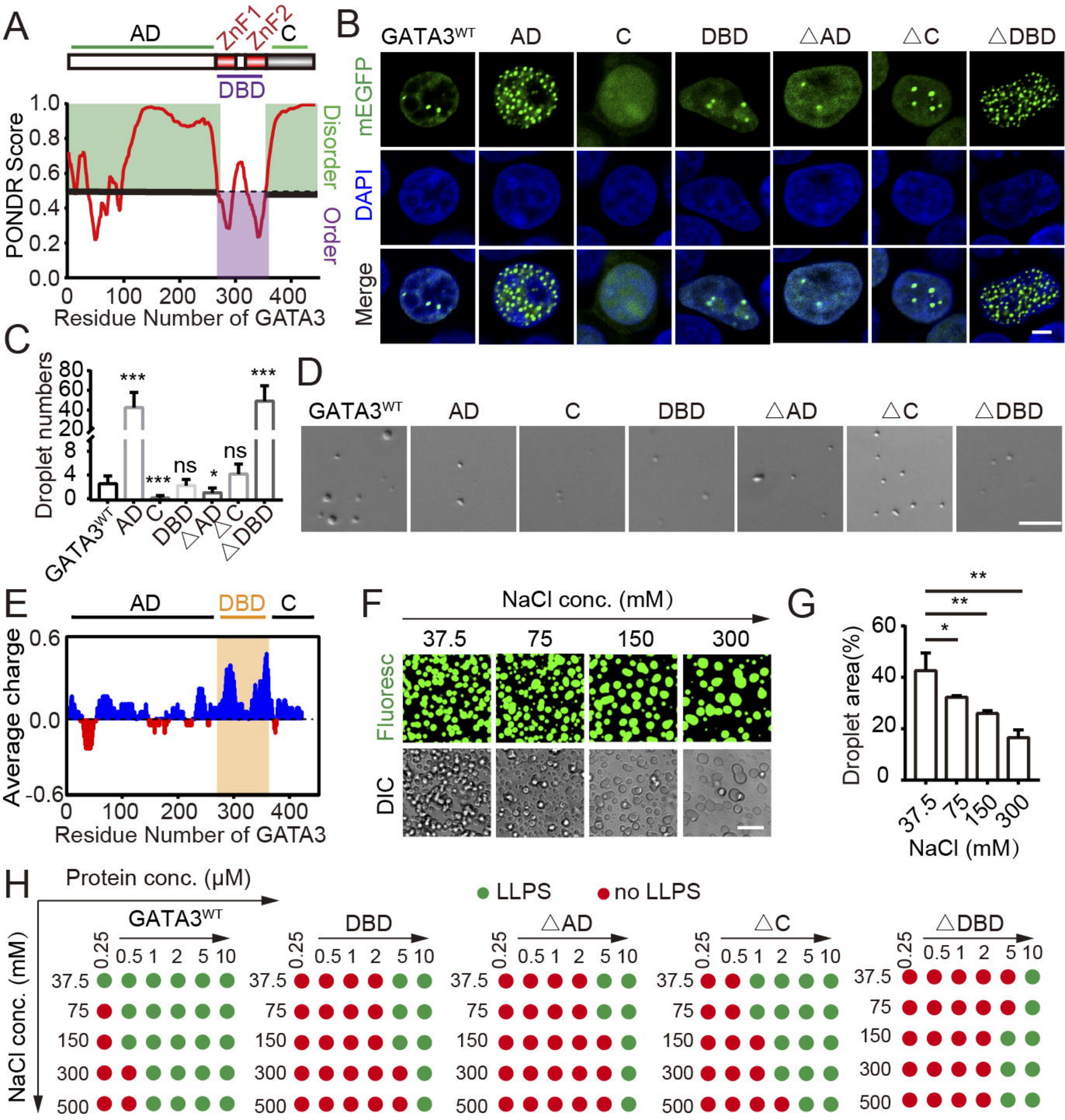
A
AD
ZnF1
ZnF2
C
DBD
PONDR Score
Disorder
Order
Residue Number of GATA3
B
GATA3WT
AD
C
DBD
△AD
△C
△DBD
mEGFP
DAPI
Merge
C
Droplet numbers
GATA3WT
AD
C
DBD
△AD
△C
△DBD
ns
D
E
Average charge
Residue Number of GATA3
F
NaCl conc. (mM)
37.5
75
150
300
Fluoresc
DIC
G
Droplet area(%)
NaCl (mM)
H
Protein conc. (μM)
LLPS
no LLPS
NaCl conc. (mM)

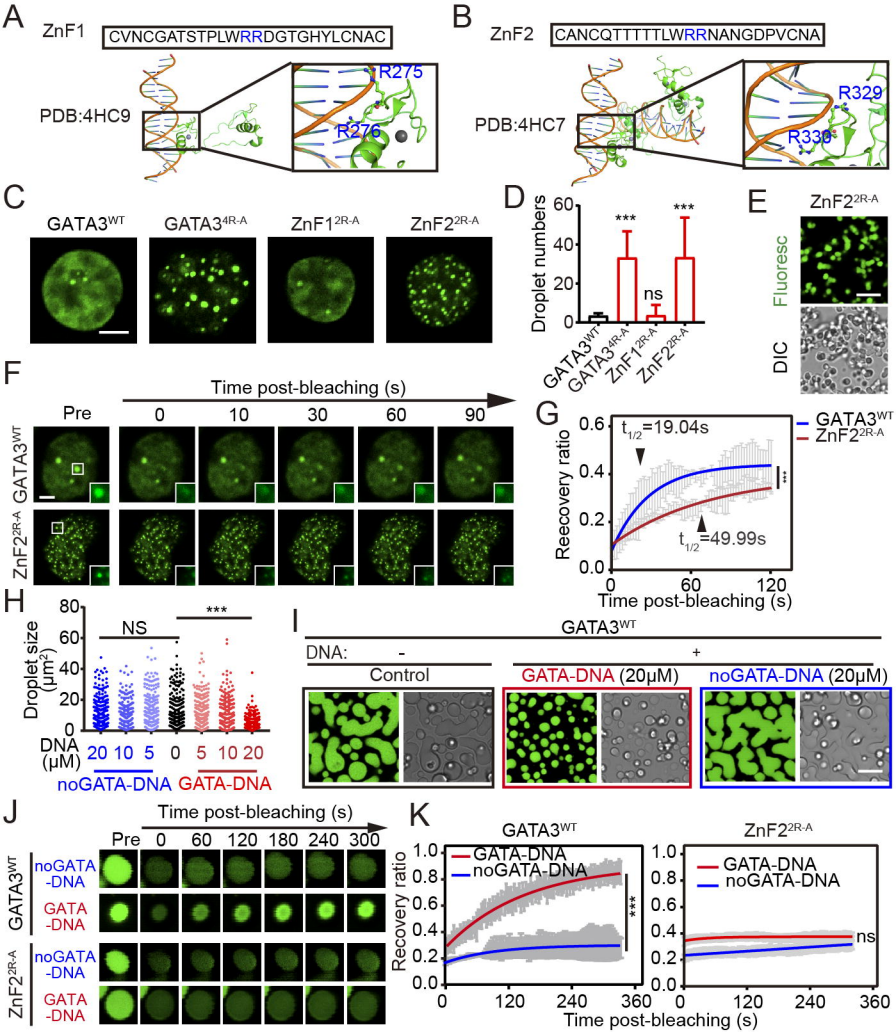
A
ZnF1
CVNCGATSTPLWRRDGTGHYLCNAC
PDB:4HC9
R275
R276
B
ZnF2
CANCQTTTTTLWRRNANGDPVCNA
PDB:4HC7
R329
R330
C
GATA3WT
GATA34R-A
ZnF12R-A
ZnF22R-A
D
Droplet numbers
***
ns
***
GATA3WT
GATA34R-A
ZnF12R-A
ZnF22R-A
E
ZnF22R-A
Fluoresc
DIC
F
Time post-bleaching (s)
Pre
0
10
30
60
90
GATA3WT
ZnF22R-A
G
Reecovery ratio
t1/2=19.04s
t1/2=49.99s
GATA3WT
ZnF22R-A
Time post-bleaching (s)
H
Droplet size (μm2)
NS
***
DNA (μM)
20 10 5 0 5 10 20
noGATA-DNA
GATA-DNA
I
GATA3WT
DNA: - +
Control
GATA-DNA (20μM)
noGATA-DNA (20μM)
J
Time post-bleaching (s)
Pre 0 60 120 180 240 300
GATA3WT
noGATA-DNA
GATA-DNA
ZnF22R-A
noGATA-DNA
GATA-DNA
K
GATA3WT
ZnF22R-A
GATA-DNA
noGATA-DNA
Recovery ratio
***
ns
Time post-bleaching (s)

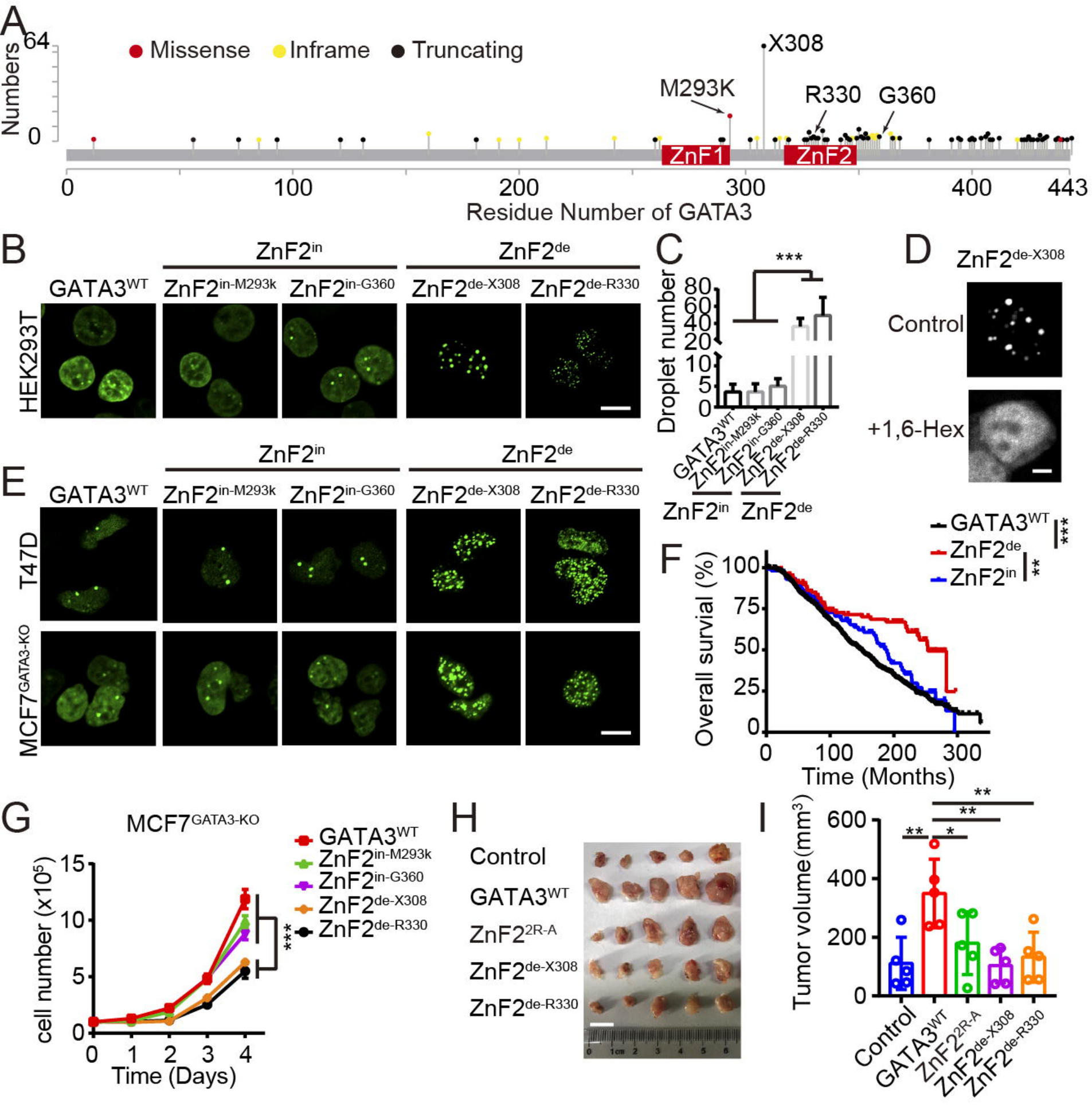
A
Missense
Inframe
Truncating
Numbers
64
0
X308
M293K
R330
G360
ZnF1
ZnF2
0
100
200
300
400
443
Residue Number of GATA3
B
ZnF2in
ZnF2de
GATA3WT
ZnF2in-M293k
ZnF2in-G360
ZnF2de-X308
ZnF2de-R330
HEK293T
C
***
Droplet number
80
60
40
20
10
5
0
GATA3WT
ZnF2in-M293k
ZnF2in-G360
ZnF2de-X308
ZnF2de-R330
ZnF2in
ZnF2de
D
ZnF2de-X308
Control
+1,6-Hex
E
ZnF2in
ZnF2de
GATA3WT
ZnF2in-M293k
ZnF2in-G360
ZnF2de-X308
ZnF2de-R330
T47D
MCF7GATA3-KO
F
GATA3WT
ZnF2de
ZnF2in
***
**
Overall survial (%)
100
75
50
25
0
0
100
200
300
Time (Months)
G
MCF7GATA3-KO
GATA3WT
ZnF2in-M293k
ZnF2in-G360
ZnF2de-X308
ZnF2de-R330
***
cell number (x10^5)
15
10
5
0
0
1
2
3
4
Time (Days)
H
Control
GATA3WT
ZnF2 2R-A
ZnF2de-X308
ZnF2de-R330
I
**
**
**
*
Tumor volume (mm3)
600
400
200
0
Control
GATA3WT
ZnF2 2R-A
ZnF2de-X308
ZnF2de-R330

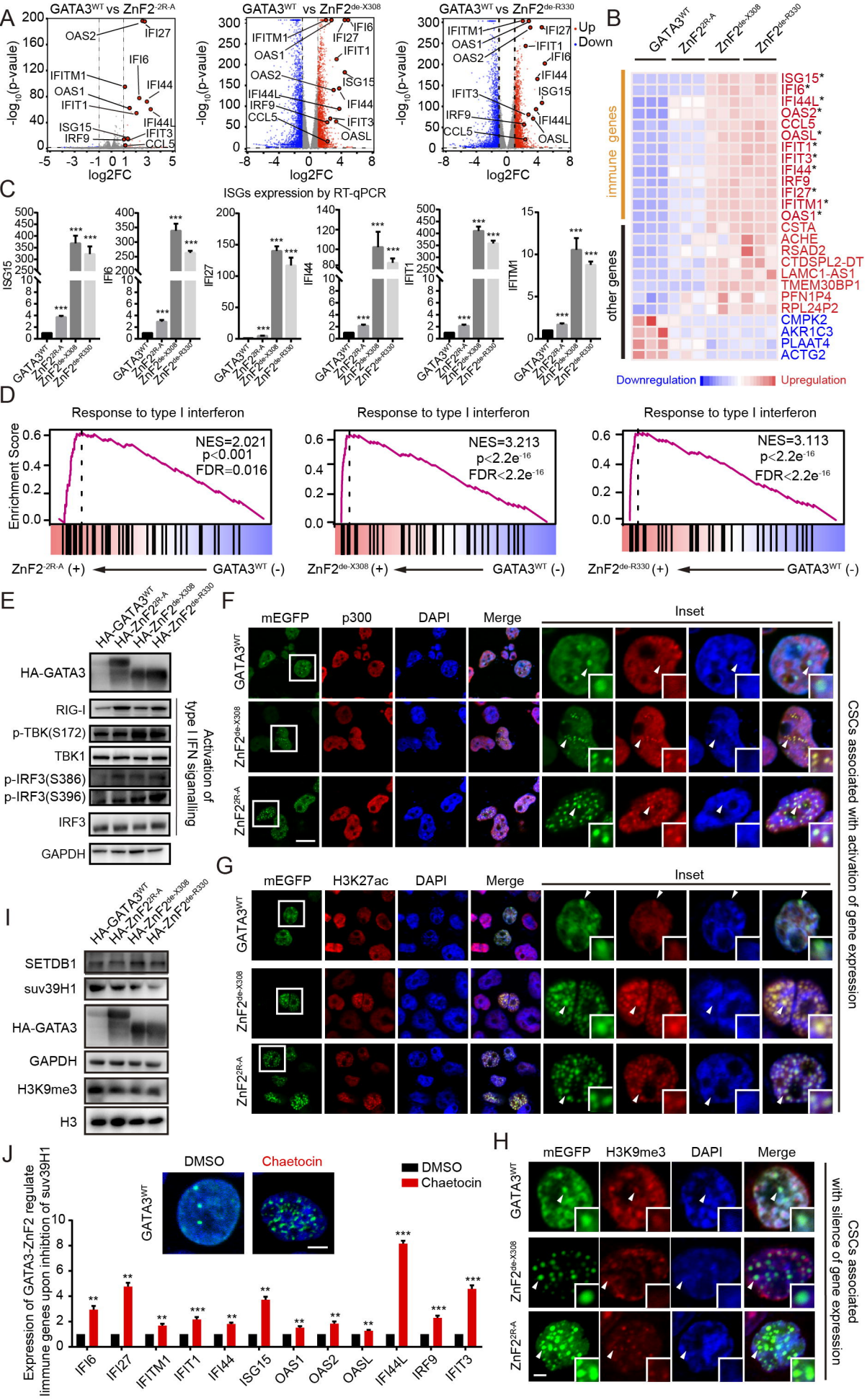
A
GATA3WT vs ZnF2-2R-A
GATA3WT vs ZnF2de-X308
GATA3WT vs ZnF2de-R330
-log10(p-vaule)
log2FC
Up
Down
OAS2
IFI27
IFI6
IFITM1
OAS1
IFIT1
IFI44
ISG15
IFI44L
IRF9
IFIT3
CCL5
OASL
B
GATA3WT
ZnF2R-A
ZnF2de-X308
ZnF2de-R330
immune genes
other genes
ISG15*
IFI6*
IFI44L*
OAS2*
CCL5
OASL*
IFIT1*
IFIT3*
IFI44*
IRF9
IFI27*
IFITM1*
OAS1*
CSTA
ACHE
RSAD2
CTDSPL2-DT
LAMC1-AS1
TMEM30BP1
PFN1P4
RPL24P2
CMPK2
AKR1C3
PLAAT4
ACTG2
Downregulation
Upregulation
C
ISGs expression by RT-qPCR
ISG15
IFI6
IFI27
IFI44
IFIT1
IFITM1
D
Response to type I interferon
Enrichment Score
NES=2.021
p<0.001
FDR=0.016
NES=3.213
p<2.2e-16
FDR<2.2e-16
NES=3.113
p<2.2e-16
FDR<2.2e-16
ZnF2-2R-A (+)
GATA3WT (-)
ZnF2de-X308 (+)
GATA3WT (-)
ZnF2de-R330 (+)
GATA3WT (-)
E
HA-GATA3WT
HA-ZnF2R-A
HA-ZnF2de-X308
HA-ZnF2de-R330
HA-GATA3
RIG-I
p-TBK(S172)
TBK1
p-IRF3(S386)
p-IRF3(S396)
IRF3
GAPDH
Activation of type I IFN siganalling
F
mEGFP
p300
DAPI
Merge
Inset
GATA3WT
ZnF2de-X308
ZnF2R-A
CSCs associated with activation of gene expression
G
mEGFP
H3K27ac
DAPI
Merge
Inset
GATA3WT
ZnF2de-X308
ZnF2R-A
I
HA-GATA3WT
HA-ZnF2R-A
HA-ZnF2de-X308
HA-ZnF2de-R330
SETDB1
suv39H1
HA-GATA3
GAPDH
H3K9me3
H3
J
DMSO
Chaetocin
GATA3WT
Expression of GATA3-ZnF2 regulate immune genes upon inhibition of suv39H1
IFI6
IFI27
IFITM1
IFIT1
IFI44
ISG15
OAS1
OAS2
OASL
IFI44L
IRF9
IFIT3
H
mEGFP
H3K9me3
DAPI
Merge
GATA3WT
ZnF2de-X308
ZnF2R-A
CSCs associated with silence of gene expression